RSC Advances

ROYAL SOCIETY OF CHEMISTRY

www.rsc.org/advances

Journal Name

COMMUNICATION

Hydroxyl-rich nanoporous carbon nanosheets synthesized by a one-pot method and their application in the in-situ preparation of well-dispersed Ag nanoparticles

Received 00th January 20xx,
Accepted 00th January 20xx

DOI: 10.1039/x0xx00000x

www.rsc.org/

Xiaodi Guo, Gaili Liu, Shuang Yue, Jing He, and Lianying Wang*

Functional nanoporous carbon nanosheets (CNSs) with high surface area have been synthesized by pyrolysis of simple organic-inorganic layered zinc hydroxides nanosheets. The synthesized CNSs with abundant hydroxyl groups display remarkable reactivity and the capability for in situ loading with ultrafine Ag NPs, which show excellent catalytic activity toward the reduction of 4-nitrophenol (4-NP) by $NaBH_4$.

Nanoporous carbon materials with high surface area and large pore volume have been widely applied in many fields such as adsorbents, catalysts supports, and electrode materials.1 To date, extensive methods (including arc-discharge,2a laser ablation,2b chemical vapour decomposition,2c and chemical or physical activation methods2d) have been employed to prepare carbon materials. Recently, carbonization of the metal–organic frameworks (MOFs) or porous coordination polymers (PCPs) is an effective way to prepare NPC due to its simplicity and high yield.3 However, most of the reported procedures involve expensive reagents (organic solvent, additional carbon sources, surfactant and templates) or complex manipulations and equipment. Therefore, it is highly desirable to develop a simple protocol for the fabrication low-cost, large-scale, nanoporous carbon materials for their large scale applications.

As efficient and cost-effective noble metal, silver nanoparticles (Ag NPs) have been attracted tremendous attention in recent years because of their unusual physical and chemical properties compared to bulk metal and their potential applications in electronic or optical materials, as well as in catalysis.4 It is well known that the overall performance of Ag NPs depend heavily upon the size, shape, dispersion. However, due to their high surface area to volume ratio, Ag NPs are typically unstable and tend to sinter into larger species, which results in a dramatic decrease in catalytic activity and selectivity. To avoid aggregation, considerable efforts have been made by immobilizing Ag NPs on/into various solid supports.5 Among a wide variety of supports, carbon materials (e.g. carbon nanofibers, graphene and carbon nanotubes) are attractive candidates for supports because of their fascinating features such as high specific surface area, good chemical and thermal stability, and intrinsic high electrical conductivity.6 It is known that preformed carbons are poor in functional groups and loading carbon supports with Ag NPs requires pre-treatment of the carbons for chemical activation or functionalization followed by the addition of a reducing agent.7 Therefore, it is highly desirable to develop a simple, cost-effective, and green strategy to synthesize Ag/carbon with well–dispersed Ag NPs embedded in the carbon matrix.

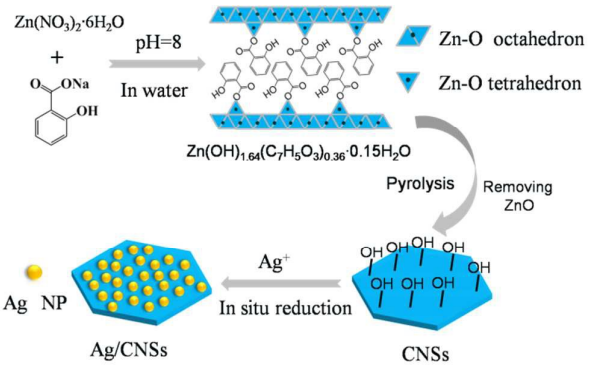

Scheme 1 Schematic illustration of the synthetic route used to synthesize hydroxyl-rich nanoporous CNSs with high surface area from organic–inorganic layered zinc hydroxides nanosheets and their application in the in-situ preparation of well-dispersed Ag nanoparticles.

Here, we demonstrate that CNSs with high surface area, large pore volume and functionality have been successfully synthesized by using the simple organic-inorganic layered zinc hydroxides nanosheets as precursor (Scheme 1). The synthesized CNSs with abundant hydroxyl groups display remarkable reactivity and the capability for in situ loading with

State Key Laboratory of Chemical Resource Engineering, Beijing University of Chemical Technology, Beijing, 100029, P. R. China
Email: 2012400142@grad.buct.edu.cn; Tel: +8610 64451027
Electronic Supplementary Information (ESI) available: Experimental details, Schematic illustration, XRD, SEM, TG-DTA, EDX, Raman spectrum, XPS spectra, , and Pore characteristics of the obtained nanoporous CNSs.See
DOI: 10.1039/x0xx00000x

ultrafine Ag NPs without the need for any external reducing agents or surface modification. We also demonstrate that the Ag NPs embedded in CNSs (Ag/CNSs) show excellent catalytic activity toward the reduction of 4-nitrophenol (4-NP) by $NaBH_4$. The layered zinc hydroxides intercalated with salicylate anions (LZHs–Sal) precursor was prepared by coprecipitation in water, which facilitates the large-scale synthesis of LZHs–Sal precursor (Details of the experimental are given in the ESI†). The X-ray diffraction (XRD) pattern (Fig. S1) of precursor exhibits the typical pattern of a layered structure with very well-ordered (00l) basal peaks at low angle, confirming the successful intercalation of salicylate anions, and the structure is similar to $Co(OH)_{1.7}(C_6H_5COO)_{0.3}\cdot 0.6H_2O$ nanoplates.8 Scanning electron microscopy (SEM) image (Fig. S2) shows the expected uniform platelet morphology. The EDX spectra (Fig. S3) shows the presence of Zn, O, C (with additional Pt signals arising from the Pt coating). Based on the elemental analysis and TG-DTA results (Fig. S4), the chemical composition of the LZHs–Sal can be written as $Zn(OH)_{1.64}(C_7H_5O_3)_{0.36}\cdot 0.15H_2O$ (Anal. Calcd: C 20.81, H 2.57%. Found: C 20.80, H 2.65%).

The LZHs–Sal was directly carbonized at 600, 700, 800, and 900°C for 5h under N_2 flow. Powder X-ray diffraction patterns (XRD) of products carbonized below 900°C are shown in Fig.S5a, where all the peaks are attributed to the ZnO deriving from the decomposition of the LZHs–Sal precursor.9 Carbon signals can be observed after removing of ZnO (Fig. S5b). However, for the samples obtained by carbonizing at 900 °C, signals of ZnO species cannot be found in the XRD pattern (Fig. S5b). This phenomenon has been explained in previous literatures.10 The XRD patterns for the four NPC samples display two broad peaks at 2θ =23° and 44°, corresponding to the diffractions for carbon.

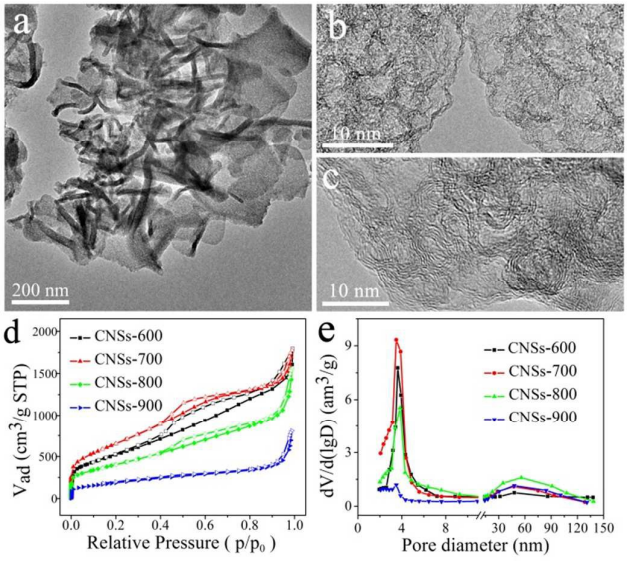

Fig. 1 (a) Low- magnification TEM image of CNSs-600, (b) HRTEM image of CNSs-600, (c) HRTEM image of CNSs-900, (d) Nitrogen adsorption–desorption isotherms and (e) pore size distributions of CNSs.

TEM image demonstrates that the carbon materials still remain the sheet–like morphology with their thickness about 25 nm, and such nanosheets are composed of interconnected structures of hollow carbon shells (4–6 nm) comprised of few graphitic carbon layers (Fig. 1a-c). Their variat ional textures revealed that the structures of the resultant carbon materials could be tuned by reasonably changing the calcination temperature. The graphitic nature of NCNSs is evident in the Raman spectra shown in Fig S6. The spectra exhibits D and G bands centered at 1342 and 1604 cm^{-1}, respectively, corresponding to the disordered carbon structures and the vibration mode to the movement in opposite directions of two carbon atoms in a single grapheme sheet.11 The appearance of G and D bands in the samples further confirms the formation of graphitic carbon, which is well consistent with the HRTEM observation.

Nitrogen adsorption-desorption isotherms are shown in Fig. 1d with the related parameters listed in Table S1. The general shape of the N_2 sorption isotherms for all the carbon nanosheets suggests the existence of different pore sizes. Especially, the steep increase in the adsorbed volume at low relative pressure reveals the presence of the micropores in the samples, and the following small slope observed at medium relative pressure as well as the desorption hysteresis demonstrates the existence of mesopores. With the increase in the carbonization temperature, the BET surface areas and the volume firstly increase and following decrease. The CNSs-700 possesses the highest surface area (2402 $m^2\cdot g^{-1}$) and the largest pore volume (2.75 $cm^3\cdot g^{-1}$), while the BET surface area of CNSs-900 decreases drastically to 667 $m^2\cdot g^{-1}$ due to the collapse of the nanoporous structure caused by graphitization.12 Pore size distributions of the four nanoporous carbon samples calculated from the nitrogen nitrogen adsorption branches are shown in Fig. 1e, the majority of pores are located in the region of mesopore. All the sampes display very close pore size distribution with a peak centering at ca. 3.8 nm.

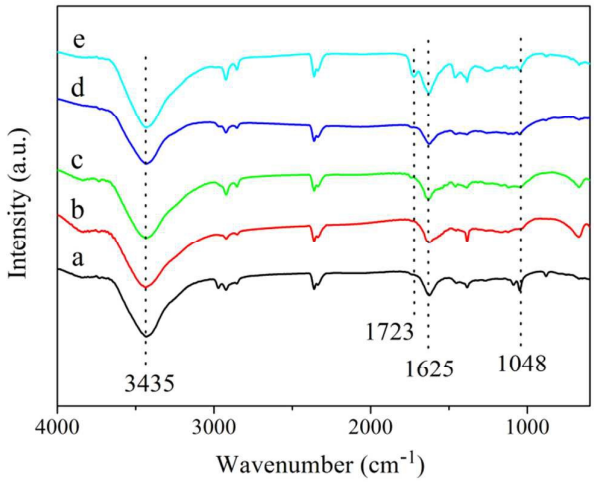

Fig. 2 FTIR spectra of (a) CNSs-600, (b) CNSs -700, (C) CNSs -800, (d) CNSs -900, and (e) Ag/CNSs nanocomposites.

Fig. 2 shows the FTIR spectrum of the as-obtained carbon nanosheets. The strong O–H stretching band at 3435 cm^{-1}, the O–H bending vibration at 1625 cm^{-1} as well as the C–O stretching bands at 1048 cm^{-1}, all of which are characteristic of hydroxyl groups. 13 Taking the hydroxyl groups of the C–900 without acidic treatment into account, we can conclude that the rich hydroxyl groups in the carbon nanosheets obtained below 900°C are derived from the functional groups of salicylate anions rather than acidic oxidation.14

Encouraged by the high surface area, large pore volume, highly graphitic degree, and rich hydroxyl groups of the graphitic carbon nanostructures, we investigated whether the obtained NCNSs can be utilized as support to prepare highly dispersed Ag NPs. The XRD pattern (Fig. S7)of the as-prepared products show that all peaks can be indexed fo fcc Ag, indicating that the Ag^+ ions have been in situ reduced without any external reducing agent.15 A comparative study of the functional groups before and after reaction with $AgNO_3$ was performed using the FTIR spectrum and XPS (Fig. S9). The FTIR spectrum of the obtained Ag/CNSs is almost the same as that of CNSs (Fig. 2). However, there is a absorption peak located at 1723 cm^{-1}, which is assigned to the carbonyl groups(C=O), indicating that hydroxyl groups in the CNSs can reduce Ag^+ to form Ag NPs and convert into carbonyl groups after reaction.16 Well-defined peaks are observed at 368.2 and 374.3 eV for Ag $3d_{5/2}$ and Ag $3d_{5/2}$(Fig. S9a), corresponding to metallic Ag^0.17 The intensity of the hydroxyl group binding energy decreased and the intensity of the carbonyl group binding energy increased after reaction(Fig. S9b-c), which is in agreement with FTIR characterization and other reports.16b It is worth noting that the binding energy of elemental O in the 1s region was higher than that of pure O, which should be ascribed to the electron transfer from O to Ag, indicative of the strong O– Ag interaction. These results reflect that hydroxyl groups were involved in the reduction of Ag^+ to form Ag^0 and the hydroxyl groups transformed into the carbonyl groups or carboxyl groups finally. Meanwhile, strong O–Ag interaction was formed, which is very important for preventing the aggregation of the Ag NPs and making the Ag NPs hard to detach from the carbon support (improving the stability). Furthermore, in the Raman spectroscopy, the intensity of the D-band and G-band for CNSs has been enhanced significantly after loading of Ag NPs (Fig. S6e), which arises from the increased Raman scattering cross sections of high–density metallic nanogaps.7e

Transmission electron microscopy (TEM) and scanning transmission electron microscopic (STEM) imaging have been used to characterize the dispersion and size of the as-synthesized Ag NPs. Except for a small percentage of Ag NPs (10 nm) on the surface of the CNSs, the vast majority of Ag NPs are uniformly embedded inside the CNSs matrix even if the Ag content is up to ~49.4 wt % (Fig. S10), indicating an excellent confinement that can avoid sintering. This could be more clearly observed in the STEM image. The EDX mappings of Ag, C, and O elements were almost overlapped, and the NPs uniformly distributed in the whole nanosheets are demonstrated to be mainly Ag NPs. Most of the Ag NPs are with a size of 2 nm. In the formation process, the CNSs served

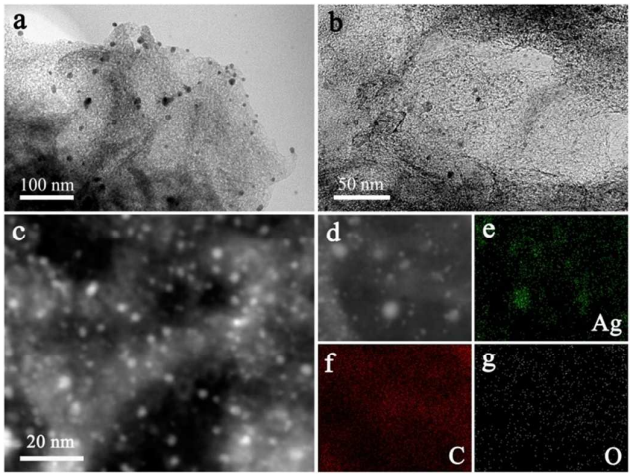

Fig. 3 (a-b) TEM images, (c-d) High-angle annular dark-field (HAADF)-STEM image, and Ag, C, and O mappings (e–g) of the Ag/CNSs nanocomposites.

not only as supports for Ag loading but also as reducing agents for reducing of Ag^+ to form Ag NPs because of the rich hydroxyl group in the CNSs possess remarkable reducing ability for in situ loading with noble metal NPs. Furthermore, it is believed that hydroxyl group with reducibility are uniformly distributed both on the surface and inside the CNSs matrix.18 Due to the large surface area and noaoporous structure, the Ag+ ions could diffuse into the interior of carbon nanosheets freely and then were reduced to Ag NPs, which were stabilized by the surrounding carbon matrix.

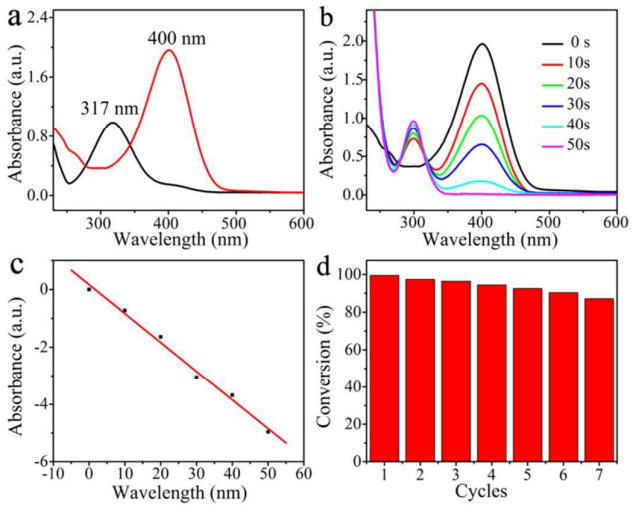

Fig. 4s (a) UV-vis spectra of 4–NP before and after adding NaBH4 solution, (b) the reduction of 4–NP in aqueous solution using Ag/ CNSs, (c) the relationship between ln (C_t/ C_0) and reaction time, and (d) Conversion of 4-NP in seven successive cycles of reduction

The catalytic properties of the Ag/CNSs nanocomposites were evaluated by the reduction of 4–nitrophenol (4-NP) to 4-aminophenol (4-AP) with excess of $NaBH_4$ as a model system, which is one of the typical model reaction for investigating the catalytic activity of metal nanoparticles. The catalytic process

of their reaction was monitored by UV-vis spectroscopy, as shown in Fig. 4, it is seen that an absorption peak of 4-NP undergoes a red shift from 317 to 400 nm immediately due to the addition of aqueous solution of $NaBH_4$, corresponding to a significant change in solution color from light yellow to deep yellow due to formation of 4–nitrophenolate ions in alkaline solution. The reaction does not proceed for a couple of days even with a large excess of $NaBH_4$ in the absence of the catalyst. When a trace amount of catalysts were added into the system, the absorption peak of 4–NP at 400 nm gradually decreases with the increase of reaction time. Meanwhile, new peak of 4-AP at 300 nm appear with their intensity increasing with time, indicating the conversion of 4-NP to 4-AP.

In the reduction process, as excess $NaBH_4$ was used, the BH_4^- concentration can be considered as a constant throughout the reaction. The ratio of C_t and C_0, where C_t and C_0 are 4-NP concentrations at time t and 0, respectively, was measured from the relative intensity of the respective absorbances, A_t/A_0. The rate constant k can be determined from the linear plot of ln (C_t/ C_0) versus reduction time was in seconds. As expected, a good linear correlation of ln (C_t/ C_0) versus time was obtained (Fig. S5), whereby a kinetic reaction rate constant *K* over the weight of catalyst is estimated to be 33.82 s^{-1} g^{-1}, which is larger than the previously reported carbon-based metal NPs cartalysts.7d, 19 As shown in Fig. 4d, Ag/CNSs can be succerssfully recycled and reused in 7 sucessive reactions with a conversion of 87%, further suggesting an excellent stability and long life. This assumption is strongly supported by the TEM and STEM images after 7 successive recycling reductions of 4-NP (Fig. S11).

In summary, nanoporous carbon nanosheets have been synthesized by solid-state pyrolysis of simple layered zinc hydroxides nanosheets intercalated with salicylate anions. At the carbonization temperature of 700°C, the highest surface area (2402 $m^2 \cdot g^{-1}$) and the largest pore volume (2.75 $cm^3 \cdot g^{-1}$) of CNSs can be achieved. The CNSs are excellent supports for Ag NPs due to their hierarchical structure, high surface area, and abundant hydroxyl groups. The resulting Ag/CNSs with well-dispersed Ag NPs embedded in the CNSs matrix show excellent catalytic activity toward the reduction of 4-nitrophenol (4-NP) by $NaBH_4$. This procedure is simple, economical and readily amenable to scale-up and therefore has great potential for commercial applications.

Notes and references

‡Footnotes relating to the main text should appear here. These might include comments relevant to but not central to the matter under discussion, limited experimental and spectral data, and crystallographic data.

c.

1 (a) Y. Liu, X. Xu, M. Wang, T. Lu, Z. Sun and L. Pan, *Chem. Commun.*, 2015, **51**, 12020; (b) K. J. Lee, Y. J. Sa, H. Y. Jeong, C. W. Bielawski, S. H. Joo and H. R. Moon, *Chem. Commun.*, 2015, **51**, 6673; (c) X. Fan, C. Yu, J. Yang, Z. Ling, C. Hu, M. Zhang and J. Qiu, *Adv. Energy Mater*., 2014, 1401761; (d) A. La Torre, M. del C. Giménez-López, M. W. Fay, G. A. Rance, W. A. Solomonsz, T. W. Chamberlain, P. D. Brown and A. N. Khlobystov, *ACS Nano*, 2012, **6**, 2000; (e) K. Xie, X. Qin, X. Wang, Y. Wang, H. Tao, Q. Wu, L. Yang and Z. Hu, *Adv. Mater.*, 2012, **24**, 347.

2 (a) Y. Saito and T. Matsumoto, *Nature*, 1998, **392**, 237; (b) A. Thess, R. Lee, P. Nikolaev, H. J. Dai, P. Petit, J. Robert, C. H. Xu, Y. H. Lee, S. G. Kim, A. G. Rinzler, D. T. Colbert, G. E. Scuseria, D. Tomanek, J. E. Fischer and R. E. Smalley, *Science*, 1996, **273**, 483; (c) Y. Xia and R. Mokaya, *Adv. Mater.*, 2004, **16**, 886; (d) J. Wang and S. Kaskel, *J. Mater. Chem*., 2012, **22**, 23710.

3 (a) B. Liu, H. Shioyama, T. Akita and Q. Xu, *J. Am. Chem. Soc.*, 2008, **130**, 5390; (b) H. Jiang, B. Liu, Y. Lan, K. Kuratani, T. Akita, H. Shioyama, F. Zong and Q. Xu, *J. Am. Chem. Soc.*, **2011**, 133, 11854; (c) L. Radhakrishnan, J. Reboul, S. Furukawa, P. Srinivasu, S. Kitagawa and Y. Yamauchi, *Chem. Mater.*, 2011, **23**, 1225; (d) S. J. Yang, T. Kim, J. H. Im, Y. S. Kim, K. Lee, H. Jung and C. R. Park, *Chem. Mater.*, 2012, **24**, 464; (e) S. Lim, K. Suh, Y. Kim, M. Yoon, H. Park, D.l N. Dybtsev and K. Kim, *Chem. Commun.*, 2012, **48**, 7447; (f) W. Chaikittisilp, M. Hu, H. Wang, H.-S. Huang, T. Fujita, K. C.-W. Wu, L.-C. Chen, Y. Yamauchi and K. Ariga, *Chem. Commun.*, 2012, **48**, 7259; (g) W. Chaikittisilp, K. Ariga and Y. Yamauchi, *J. Mater. Chem. A*, 2013, **1**, 14; (h) K. Xi, S. Cao, X. Peng, C. Ducati, R. V. Kumar and A. K. Cheetham, *Chem. Commun.*, 2013, **49**, 2192; (i) N.L. Torad, M. Hu, Y. Kamachi, K. Takai, M. Imura, M. Naito and Y. Yamauchi, *Chem. Commun.*, 2013, **49**, 2521; (j) Y. Liu, X. Xu, M. Wang, T. Lu, Z. Sun L. Pan, *Chem. Commun.*, 2015, **51**, 12020; (k) J. Tang, R. R. Salunkhe, J. Liu, N. L. Torad, M. Imura, S. Furukawa and Y. Yamauchi, *J. Am. Chem. Soc.*, 2015, **137**, 1572.

4 (a) L. Maretti, P. S. Billone, Y. Liu and J. C. Scaiano, *J. Am. Chem. Soc.*, 2009, **131**, 13972; (b) J. Park, D.-H. Lim, H.-J. Lim, T. Kwon, J. Choi, S. Jeong, I.-H. Choi and J. Cheon, *Chem. Commun.*, 2011, **47**, 4382; (c) X. Zou, R. Silva, X. Huang, J. F. Al-Sharab and T. Asefa, *Chem. Commun.*, 2013, **49**, 382.

5 (a) R. Liu, Y.-W. Yeh, V. H. Tam, F. Qu, N. Yao and R. D. Priestley, *Chem. C ommun.*, 2014, **50**, 9056; (b) J. Liu, J. Cui, F. Vilela, J. He, M. Zeller, A. D. Hunter and Z. Xu, *Chem. Commun.*, 2015, **51**,12197; (c) S. S. Acharyya, S. Ghosh and R. Bal, *Chem. Commun.*, 2015, **51**, 5998.

6 (a) G. L. Bezemer, J. H. Bitter, H. P. C. E. Kuipers, H. Oosterbeek, J. E. Holewijn, X. Xu, F. Kapteijn, A. J. van Dillen and K. P. de Jong, *J. Am. Chem. Soc.*, 2006, **128**, 3956; (b) K. K. R. Datta, B. V. S. Reddy, K. Ariga and A Vinu, *Angew. Chem. Int. Ed.*, 2010, **49**, 5961; (c) X. Chen, G. Wu, J. Chen, X. Chen, Z. Xie and X. Wang, *J. Am. Chem. Soc.*, 2011, **133**, 3693; (d) X. Zou, X. Huang, A. Goswami, R. Silva, B. R. Sathe, E. Mikmeková and T. Asefa, *Angew. Chem. Int. Ed.*, 2014, **53**, 4372; (e) J. Li, Q-L. Zhu and Q. Xu, *Chem. C ommun.*, 2015, **51**, 10827.

7 (a) X. Lu, H. Qi, X. Zhang, Z. Xue, J. Jin, X. Zhou and X. Liu, *Chem. Commun.*, 2011, **47**, 12494; (b) B. Yu, J. Feng, S. Liu and T. Zhang, *RSC Adv.*, 2013, **3**, 14303; (c) H. Wang, J. Shen, Y. Li, Z. Wei, G. Cao, Z. Gai, K. Hong, P. Banerjee and S. Zhou, *ACS Appl. Mater. Interfaces*, 2013, **5**, 9446; (d) Y. Tian, Y. Cao, F. Pang, G. Chen and X. Zhang, *RSC Adv.*, 2014, **4**, 43204; (e) T. Gao, D. Yang , L. Ning, L. Lei, Z. Ye and G. Li, *Nanoscale*, 2014, **6**, 14828; (f) Z. Xue, F. Zhang, D. Qin, Y. Wang, J. Zhang, J. Liu, Y. Feng and X. Lu, *Carbon*, 2014, **69**, 481; (g) W. Shao, X. Liu, H. Min, G. Dong, Q. Feng and S. Zuo, *ACS Appl. Mater. Interfaces*, 2015, **7**, 6966.

8 X. Guo, L. Wang, S. Yue, D. Wang, Y. Lu, Y. Song and J. He, *Inorg. Chem.*, 2014, **53**, 12841.

9 S. Cho, J.-W. Jang, K. Kong, E. S. Kim, K.-H. Lee and J. S. Lee, *Adv. Funct. Mater.*, 2013, **23**, 2348.

10 (a) B. Liu, H. Shioyama, H. Jiang, X. Zhang and Q. Xu, Carbon, 2010, 48, 456; (b) J. Hu, H. Wang, Q. Gao and H. Guo, *Carbon*, 2010, **48**, 3599.

11 P. Zhang, F. Sun, Z. Xiang, Z. Shen, J. Yun and D. Cao, *Energy Environ. Sci.*, 2014, **7**, 442.
12 M. Hu, J. Reboul, S. Furukawa, N. L. Torad, Qi. Ji, P. Srinivasu, K. Ariga, S. Kitagawa and Y. Yamauchi, *J. Am. Chem. Soc.*, 2012, **134**, 2864.
13 Q. Li, B. Guo, J. Yu, J. Ran, B. Zhang, H. Yan and J. R. Gong, *J. Am. Chem. Soc.*, 2011, **133**, 10878.
14 S. Yang, L. Wang, S. Yue, X. Guo, Y. Song and J. He, *RSC Adv.*, 2013, **3**, 16990.
15 C.-H. Hsia, M.-Y. Yen, C.-C. Lin, H.-T. Chiu and C.-Y. Lee, *J. Am. Chem. Soc.*, 2003, **125**, 9940
16 (a) X. Sun and Y. Li, *Angew. Chem. Int. Ed.*, 2004, **43**, 597; (b) Q. Lu, J. Deng, Y. Hou, H. Wang, H. Li, Y. Zhang and S. Yao, *Chem. Commun.*, 2015, **51**, 7164; (c) Y. Zhuo, D. Zhong, H. Miao and X. Yang, *RSC Adv.*, 2015, **5**, 32669.
17 (a) L. Shen, M. Chen, L. Hu, X. Chen and J. Wang, *Langmuir*, 2013, **29**, 16135; (b) Y. Chen, T. Yang, H. Pan, Y. Yuan, L. Chen, M. Liu, K. Zhang, S. Zhang, P. Wu and J. Xu, *J. Am. Chem. Soc.*, 2014, **136**, 1686.
18 H.-W. Liang, W.-J. Zhang, Y.-N. Ma, X. Cao, Q.-F. Guan, W.-P. Xu and S.-H. Yu, *ACS Nano*, 2011, **5**, 8148.
19 (a) Z. Ji, X. Shen, G. Zhu, H. Zhou and A. Yuan, *J. Mater. Chem.*, 2012, **22**, 3471; (b) Y. Yang, Y. Ren, C. Sun and S. Hao, *Green Chem.*, 2014, **16**, 2273.

Hydroxyl-rich nanoporous carbon nanosheets synthesized by a one-pot method and their application in the in–situ preparation of well-dispersed Ag nanoparticles

Xiaodi Guo, Gaili Liu, Shuang Yue, Jing He, and Lianying Wang*

Functional nanoporous carbon nanosheets (CNSs) with high surface area have been synthesized by pyrolysis of simple organic-inorganic layered zinc hydroxides nanosheets. The synthesized CNSs with abundant hydroxyl groups display remarkable reactivity and the capability for in situ loading with ultrafine Ag NPs, which show excellent catalytic activity toward the reduction of 4-nitrophenol (4-NP) by $NaBH_4$.